Isogenic human iPSC pairs reveal a neuronal subtype-specific and genetic background-independent mechanism of *SCN1A* epilepsy

Authors:

Yunyao Xie[1], Nathan N. Ng[1, #a], Olga S. Safrina[1], Carmen M. Ramos[1], Kevin C. Ess[2], Philip H. Schwartz[3], Martin A. Smith[4], Diane K. O'Dowd[1]*

[1] Department of Developmental and Cell Biology, University of California, Irvine, Irvine, CA

[2] Department of Pediatrics, Vanderbilt University Medical Center, Nashville, TN

[3] Children's Hospital of Orange County Research Institute, Orange, CA.

[4] Department of Anatomy and Neurobiology, University of California, Irvine, Irvine, CA

[#a] Current Address: Stanford University, School of Medicine, Stanford, CA 94305

***Correspondence Address:**

Diane K. O'Dowd

4221 McGaugh Hall, University of California, Irvine

Irvine, CA 92697

Phone: +1 (949) 824-8141

Email: dkodowd@uci.edu

Abstract:

Over 1250 mutations in *SCN1A,* the voltage-gated sodium channel gene Nav1.1, are associated with seizure disorders including GEFS+ and Dravet Syndrome (DS). To evaluate how a specific mutation, independent of genetic background, causes seizure activity we generated two pairs of isogenic human iPSC lines by CRISPR/Cas9 gene editing. One pair is a control line from an unaffected sibling, and the mutated control carrying the GEFS+ K1270T *SCN1A* mutation. The second pair is a GEFS+ patient line with the K1270T mutation, and the corrected patient line. By comparing the electrophysiological properties in inhibitory and excitatory iPSC-derived neurons from these pairs, we found the K1270T mutation causes gene dosage-dependent and cell type-specific alterations in sodium current density and evoked firing, resulting in hyperactive neural networks. We also identified differences associated with genetic background and interaction between the mutation and genetic background. Dual isogenic iPSC-derived neuronal cultures provide a novel platform for developing patient-specific anti-seizure therapies.

Genetic epilepsy with febrile seizure plus (GEFS+) is a form of epilepsy with febrile seizures that persists beyond six years of age[1]. The clinical phenotype of GEFS+ is variable but affected individuals characteristically have mild febrile seizures or febrile seizure plus (FS+) in early childhood, followed by tonic, clonic, myoclonic, or absence seizures in late childhood[2]. Mutations in several genes including *SCN1A*, *SCN1B*, *SCN2A*, *GABRG2*, and *GABRD* can cause GEFS+[3–12]. One hot spot for mutations causing GEFS+ is the *SCN1A* gene which encodes the alpha subunit of the Nav1.1 voltage-gated sodium channel. Approximately 50 missense mutations at locations throughout *SCN1A* are associated with GEFS+[13]. There are also multigenerational families in which individuals with the same *SCN1A* mutation exhibit a broad range of seizure phenotypes[14,15]. The heterogeneity of disease phenotypes arising from different mutations in the same gene, and from the same mutation between individuals complicates understanding of the underlying cellular mechanisms of *SCN1A* epilepsy. Model systems that aid in mapping the links between individual *SCN1A* mutations and their cellular effects can facilitate development of more effective patient-specific drug therapies. Zebrafish, knock-in *Drosophila* and mouse models have all been important tools in this endeavor[16] but evolutionary distances leading to species-specific mechanisms may lead to failed therapies in patients[17,18].

In recent years, patient-derived induced pluripotent stem cells (iPSCs) that can be differentiated into neurons have emerged as a new model to explore how epilepsy-associated *SCN1A* mutations affect activity and sodium channel properties in human neurons. These studies have focused on mutations associated with Dravet syndrome (DS), a form of epilepsy that is typically more severe that GEFS+. Previous studies in iPSC-derived neurons have shown that nonsense R1645X, and missense S1328P and Q1923R mutations in *SCN1A* confer impaired excitability and reduced sodium current density in inhibitory neurons, giving rise to hyperactivity in neural networks[19–21]. Examination of missense Q1923R and F1415I *SCN1A* mutations shows increased excitability, epileptic activity, and sodium current amplitudes in excitatory neurons[22]. Interestingly, the IVS14+3A>T mutation which causes truncation of DIIS2 and

S3 of Nav1.1 affects both excitatory and inhibitory neurons[23].

In addition to alterations caused by discrete mutations, differences in genetic background represent a major source of variability that complicates interpretation of any experimental findings as they can influence phenotypic differences[24,25]. Evaluation of a large cohort of control and patient iPSC lines can help assess the contribution of mutations to disease phenotypes[26]. However, a more direct way to examine the effect of a mutation independent of genetic background is to compare the cellular changes caused by a single mutation in isogenic pairs of control and mutant iPSC lines[20,26–29]. A recent study of DS-associated *SCN1A* Q1923R mutation used transcription activator-like effector nucleases (TALENs) to generate an isogenic corrected line by correcting the *SCN1A* mutation[20]. Comparison of the isogenic corrected versus the patient line revealed a decrease in sodium current density in the patient line. Comparison of the isogenic corrected line with a control line from a different genetic background revealed additional alterations in the voltage dependence of Nav activation and AP threshold suggesting these might be associated with the genetic background of the patient. An isogenic mutant line in which the mutation has been introduced into the control would provide additional insight into the origin of these differences.

In the current study both isogenic corrected and mutant iPSC lines were generated via CRISPR/Cas9 editing. These were used to assess the contribution of the autosomal dominant *SCN1A* K1270T mutation identified in a GEFS+ family to the etiology of the disease[14]. Two isogenic pairs of iPSC lines were used: 1a) control (unaffected sibling), 1b) mutated control, and 2a) patient with K1270T *SCN1A* mutation (GEFS+ sibling), 2b) corrected patient. These two pairs of isogenic iPSC lines can be differentiated into functional mixed neuronal cultures that contain both GABAergic and glutamatergic neurons. Comparison of electrophysiological properties of neurons within and between pairs identified mutation-dependent alterations independent of genetic background. There were also differences found to be associated with the genetic background or interactions between the mutation and the background. Such CRISPR/Cas9-based disease modeling strategy with isogenic pairs of

iPSC-derived neurons represents a promising platform for developing patient-specific therapies based on disease mechanisms.

1. Methods

1.1 Preparation and maintenance of hiPSCs

Skin fibroblasts were collected from two male siblings of the GEFS+ family by K.E. (Vanderbilt University Medical Center) after obtaining informed consent using IRB approved protocol #080369. The control fibroblast donor had no known clinical diagnoses; the patient sibling had four febrile seizures in total since half a year old and four generalized atypical absence seizures since the age of two[14]. Age at time of biopsy was 23 years (control) and 21 years (patient).

Skin fibroblasts were reprogrammed into iPSCs by the Schwartz laboratory as published[30]. Two human iPSC lines were generated, SC210.12-SF6-2I3.M11S8 (control) and SC215.19-SF4-2I8.M10S6 (patient). iPSCs were maintained in feeder-free conditions following published protocols[30,31].

1.2 CRISPR/Cas9 editing on iPSCs derived from two siblings

To generate a mutated control line, the K1270T mutation was knocked into an iPSC line generated from the unaffected sibling (SC210.12-SF6-2I3-M11S8-S4-S6-S2). The 20-nt guide RNA (sgRNA) 5'-CTTCTAAAATGGGTGGCATA-3' was designed using the CRISPR design tool (http://crispr.mit.edu) from the Zhang laboratory and cloned into plasmid pSpCas9(BB)-2A-Puro (Px459) V2.0 (Addgene, 62988). Plasmid constructs were purified with the Endo-free Plasmid Maxiprep kit (Qiagen). The 140-nt repair template ssODN1 5'-GATTAAGACGATGTTGGAATATGCTGACAAGGTTTTCACTTACATTTTCATTCTGGAAATGCTTCTAACATGGGTGGCATATGGATATCAAACATATTTCACCAATGCCTGGTGTTGGCTGGACTTCTTAATTGTTGATG-3' (Integrated DNA Technologies) was designed with two homologous arms flanking the Cas9 cleavage site, the threonine codon (ACA) at the mutation site and an addition of a silent EcoRV mutation.

To generate a corrected patient line, the mutation was removed from a patient iPSC line (SC215.19-SF4-2I8.M10S6-S2-S2). sgRNA (5'-CTTCTAAC

ATGGGTGGCATA-3') complementary to the target sequence of mutated allele was cloned into the same plasmid. The 140-nt repair template ssODN2 (5'-GATTAAGACGATGTTGGAATATGCTGACAAGGTTTTCACTTACATTTTCATT CTGGAAATGCTTCTAAAATGGGTGGCATATGGCTATCAAACATATTTCACC AATGCCTGGTGTTGGCTGGACTTCTTAATTGTTGATG-3') (Integrated DNA Technologies) was similar to ssODN1 but with the lysine codon at the mutation site (AAA) and without EcoRV silent mutation. 8 x 10^5 cells were co-transfected with 3 μg plasmid-sgRNA construct and ssODN (0.6 μM final concentration) with Amaxa Human Stem Cell Nucleofector Kit 1 (Lonza) and program A-023 for the Amaxa Nucleofector Device II. To obtain low seeding density, the transfected cell suspension was diluted in a 1:6 - 1:8 ratio and plated into Matrigel-coated wells of 6-well plates. 24 hours post-transfection, cells were treated with 2 μg/ml puromycin (Sigma) in StemPro complete media[31] containing 0.58 μl/ml SMC4 (Corning). 48 hours post-transfection, cells were switched to normal StemPro complete media containing 0.58 μl/ml SMC4. Continued maintenance required media that included 50% conditioned media from 70-90%-confluent unedited iPSC cultures and 50% StemPro complete media with 55 μM β-mercaptoethanol, 1×StemPro, 20 ng/ml bFGF and 0.58 μl/ml SMC4. 6-8 days post-nucleofection, isolated iPSC colonies with 20-30 cells were formed, picked manually using customized glass hooks, and transferred to single wells in 96- or 48-well plates with pre-wet 20 μl barrier micropipette tips. StemPro complete media supplemented with 0.58 μl/ml SMC4 was used for daily feeding. At 100% confluence, clones were split with pre-warmed 62 μl (96-well plate) or 125 μl (48-well plate) of Accutase (Millipore) in a 1:2 ratio. Cells were eventually expanded into two wells in a 48-well plate to be used for freezing as well as sequencing and/or restriction digestion, respectively. All media for feeding and splitting were prepared immediately prior to use and equilibrated at 37°C and 5% CO_2.

A protocol for freezing iPSCs in low density was modified from Stover *et al*[31]. Cells at 100% confluence were cryopreserved with pre-chilled freezing medium containing 40% conditioned medium from 70-90% confluent culture, 40% StemPro complete medium, 10% DMSO, 10% bovine serum albumin

(25% BSA, Gibco) with addition of 0.58 μl/ml SMC4. To increase viability of cells during defrosting, clones from 48-well plates were frozen with 50-250 μl of freezing medium depending on the size of pellets after centrifugation and were stored in 1.2 ml cryo-vials at -80°C.

Genomic DNA was extracted with 10-13 μl of QuickExtract DNA Extraction Solution (Epicentre). Fragments around the intended mutation sites were amplified by PCR in 50 μl reactions with Taq DNA polymerase (Invitrogen), forward primer 5'- CTACCATAGATTCCATCCCCCAA -3' and reverse primer 5'- TTCCACCAATAGTCTTTCCCCTG -3'. PCR products were confirmed by gel electrophoresis and purified with MinElute PCR Purification Kit (Qiagen) prior to sequencing (Retrogen). MacVector software was used to analyze sequencing data.

Additionally, a subset of mutated control clones was subject to restriction digestion by EcoRV prior to sequencing analysis. As we observed the absence of EcoRV mutation in some of the positive clones with K1270T mutation, direct sequencing was used to screen the remaining clones.

Both pairs of isogenic iPSCs were karyotyped and the *SCN1A* gene was sequenced every 20-30 passages. Cell lines at low passage were expanded for cryopreservation. Research was approved by hSCRO (#2011-1023) and IBC protocols (#2011-1377).

1.3 Differentiation of two pairs of isogenic iPSCs into neurons

Two pairs of isogenic iPSCs within 40 passages of the original generation were patterned into neurons as described[32]. Neural progenitor cells derived from iPSCs were plated on top of 50-70% confluent mouse astroglial feeder layers that were prepared following a published protocol[33].

At D17 post-plating, excitatory and inhibitory neurons were labeled by transfection with CaMKII-eGFP (Addgene, 50469) and GAD1-mCherry (Genecopoeia, HPRM15652-PM02) plasmids in MTI (GlobalStem) or ViaFect (Promega) reagents.

1.4 Immunostaining and imaging

To evaluate the expression of pluripotency markers, iPSCs were plated onto glass coverslips coated with Matrigel diluted 1:30 in DMEM/F-12 + Glutamax. iPSCs were maintained using StemPro medium (section 1.2). When grown to ~70% confluence, coverslips were fixed and stained as described[32]. Primary antibodies OCT-3/4 (1:100; Santa Cruz Biotechnology, sc-5279), SOX2 (1:100; Santa Cruz Biotechnology, sc-365823) and NANOG (1:50; Santa Cruz Biotechnology, sc-293121) were used to characterize the pluripotency of the iPSCs. 4',6-diamidino-2-phenylindole (DAPI; Life Technologies) staining was added to visualize nuclei.

iPSC-derived neurons were stained with antibodies of βIII-tubulin (1:1000; Sigma-Aldrich, T8660) and GABA (1:4000; Sigma-Aldrich, A2052) to assess the proportion of GABAergic neurons. Neurons were identified by morphology, expression of βIII-tubulin in the cell bodies and neuronal processes, and nuclear localization of DAPI.

Images were taken by a Zeiss M2 Imager fluorescence microscope and processed using the supplied Zen software.

1.5 Whole-cell recording

Whole-cell recordings were obtained from iPSC-derived inhibitory and excitatory neurons at D21-23 post-plating at room temperature. This time period was selected based on studies in two control cell lines demonstrating that a high percentage of neurons were functionally active by this age[32]. Patch pipettes were pulled from unpolished borosilicate glass (VWR International) by PC-10 (Narishige). Open tip resistance was 6-8 MΩ. External solution contained (in mM): 120 NaCl, 5.4 KCl, 0.8 $MgCl_2$, 1.8 $CaCl_2$, 15 glucose, 20 HEPES, with pH at 7.2-7.4. Osmolality was adjusted to 290 - 295 mOsm. Internal solution contained (in mM): 120 potassium gluconate, 20 NaCl, 0.1 $CaCl_2$, 2 $MgCl_2$, 1.1 EGTA, 10 HEPES, 4.5 Na_2ATP with pH at 7.2. Osmolality was around 280 - 283 mOsm. Voltages were corrected for a 5 mV junction potential. To record evoked action potentials, membrane potential was held at -75 mV by injecting sub-threshold currents and cells were depolarized by a series of current injections.

Excitatory and inhibitory postsynaptic currents (EPSCs and IPSCs) were separated at reversal potentials (-49 mV and -2 mV) with a gap-free protocol under voltage clamp. Recordings of spontaneous PSCs (sPSCs) were performed with the standard external solution and a cesium gluconate internal solution containing (in mM): 130 Cs^+ gluconate, 0.2 EGTA, 2 $MgCl_2$, 6 CsCl, 10 HEPES, 2.5 adenosine 5' triphosphate sodium salt, 0.5 guanosine 5' triphosphate sodium and 10 disodium phosphocreatine. Voltages were corrected for a 7 mV junction potential. Miniature postsynaptic currents (mPSCs) were recorded in external solution containing 1 μM tetrodotoxin (TTX; Alomone).

Isolated sodium currents were recorded with external solution containing (in mM): 120 NaCl, 5.4 KCl, 0.8 $CoCl_2$, 15 glucose, 20 HEPES, 2.5 tetraethylammonium and 1.0 4-aminopyridine. Voltages were corrected for a 10 mV junction potential. The voltage dependence of activation was determined with a step protocol. Cell membrane potential was increased from a holding potential of -100 mV to a range of potentials between -100 mV and 30 mV with a step interval of 10 mV for 45 s. Peak transient currents were plotted against holding potentials and fit with the following equation:

$$\mathrm{I} = \frac{(V-Vrev)\times Gmax}{1+\exp\left(-\frac{V-Vhalf}{k}\right)} \qquad (1)$$

where I is the peak current amplitude, V is the holding potential of each pulse, V_{rev} is the reversal potential, G_{max} is the maximal conductance, V_{half} is the voltage with 50% channels activated, and k is the slope. Conductance was calculated with the following equation:

$$\mathrm{G} = \frac{1}{V-Vrev} \qquad (2)$$

where G is conductance, and I, V, V_{rev} were as described in equation (1).

The voltage dependence of steady-state inactivation was analyzed with a two-step protocol. It began with a holding potential of -100 mV. Next the conditioning pulse was increased through a series of voltage steps from -100 mV to 30 mV with an interval of 10 mV for 90 ms. A test pulse at -10 mV for 90 ms was immediately applied and followed by a holding potential of -100 mV. The peak current amplitude during test pulses were normalized to that during

the first test pulse and then plotted against the holding potential of the conditioning pulse. The I-V curves were fitted to the following equation:

$$\mathrm{I} = \frac{1}{1+exp\frac{V-Vhalf}{k}} \qquad (3)$$

where I is the normalized peak current amplitude during the test pulses, V_{half} is the voltage with 50% channels inactivated, and k is the slope.

The recovery from steady-state inactivation was determined using a second two-pulse protocol. Following a holding potential of -100 mV for 27 ms, two test pulses at -10 mV for 90 ms were separated by a time interval with a range of 1-10 ms with an increment of 1 ms in the first protocol, and 10-50 ms with an increment of 5 ms in the subsequent protocol. Peak current amplitude from the second pulse was normalized to the average current amplitude from the first pulse to calculate the fractional recovery. The data of recovery were fitted using the following equation:

$$\mathrm{I} = \mathrm{A} \times \exp\left(-\frac{t}{\tau}\right) + B \qquad (4)$$

where I is the normalized current amplitude, A is the relative percentage of recovered currents, t is the time interval, and τ is the time constant of recovery.

Electrophysiological data were collected with a List EPC7 amplifier and a Digidata 1320A D-A converter (Axon Instruments), or a MultiClamp 700B amplifier and a Digidata 1440A D-A converter (Axon Instruments). Recordings were obtained by pClamp8 or pClamp10 (Axon Instruments) software with a Bessel filter at 2 kHz and a low-pass filter at 10 kHz.

1.6 Data Analysis and Statistics

Counting from fluorescent micrographs was conducted in a blinded fashion with respect to cell line. For each coverslip, at least 3 fields with evenly distributed cells observed via DIC were chosen for counting. 3 coverslips each from individual plating of an iPSC cell line were included for counting the number of cells expressing pluripotency markers.

Electrophysiological data were analyzed using Clampfit 10.6 (Molecular Devices). Cells that were included in electrophysiological analyses had an amplitude of leak current smaller than 50 pA at a holding potential of -75 mV.

Evoked action potentials (APs) recorded under current clamp were included if they had a stable baseline at -65 ~ -85 mV with sub-threshold current injection, a peak amplitude ≥ -5 mV on the first AP and ≥ -15 mV in subsequent APs within the train. AP events were excluded if the maximum firing frequency deviated from mean by more than ± 2SD. Rheobase data were excluded if the resting membrane potentials (RMP) were more depolarized than -35 mV. AP amplitude and half-width data were not included if the cell did not fire evoked AP. PSCs recorded under voltage-clamp were analyzed using Mini Analysis 6.0.7 (Synaptosoft). PSCs were identified as events with an amplitude ≥ 5 pA (2× RMS noise of 2.5 pA) and were then manually verified individually. Cells were excluded from sodium current analysis if their current density in the range of -10 - 40mV was 2SD beyond the mean.

Electrophysiological data are presented with n = number of recorded cells and the number of individual platings shown in parentheses. All data were analyzed with D'Agostino-Pearson normality test. Statistical tests were selected based on the normality test results and performed in Prism 7.0.2 (GraphPad Software). Figures were generated using DeltaGraph 7.1 (Red Rock Software)

2. Results

2.1. Isogenic pairs of iPSCs were generated by CRISPR/Cas9 editing

The autosomal dominant K1270T *SCN1A* mutation identified in a GEFS+ family results in a lysine-to-threonine conversion in the second transmembrane segment of the third homologous domain in the α subunit of the human Nav1.1 protein[14] (Figure 1A). Skin fibroblasts were collected from two male siblings (an unaffected control and a GEFS+ patient) and reprogrammed into iPSC lines (Figure 1B). To examine the contribution of the K1270T mutation to disease phenotypes, two pairs of isogenic lines were included in this study. In the first pair, the GEFS+ K1270T mutation (c.4227A>C) was knocked into the unaffected sibling derived control line using CRISPR/Cas9. For the second isogenic pair, the K1270T mutation in the patient line was corrected (c.4227C>A; Figure 1C). Most of the mutated control clones with desired sequence were homozygous, possibly due to the short distance (9 bp) between

the Cas9 cut site and the K1270T mutation locus[34]. The efficiency of obtaining a positive clone with desired sequence was 4-5% in both knock-in and correction lines (Table 1).

Sequencing of DNAs from four iPSC lines confirmed the presence of the K1270T mutation in two alleles in the mutated control (*SCN1A*$^{KT/KT}$) and in one allele in the patient line (*SCN1A*$^{KT/+}$), and the absence of the mutation in the control (*SCN1A*$^{+/+}$) and the corrected patient lines (*SCN1A*$^{+/+}$; Figure 1D). The engineered homozygous isogenic mutant provides a unique opportunity since two copies of *SCN1A* mutations are usually lethal to organisms *in vivo*[35,36]. Karyotypes of four iPSC lines were verified normal with 46, XY chromosomes (Figure 1E). Pluripotency of each cell line was confirmed by staining for expression of OCT-3/4, SOX2 and NANOG[37] (Figure 2A and 2B).

Table 1. Efficiency of generating isogenic mutant and corrected clones via CRISPR/Cas9 editing

	Clones sequenced	Clones w/ HDR	Het w/ desired seq	Homo w/ desired seq	Efficiency (%)
Mut ctrl	58*	7	0	3	5.2
Corr pt	147	31	-	6	4.1

Efficiency was calculated by # clones with desired sequence / # clones sequenced. Mut ctrl, corr pt, HDR, het and homo are abbreviated for mutated control, corrected patient, homology directed repair, heterozygous and homozygous respectively.
* 58 isogenic mutant clones were analyzed by sequencing and/or EcoRV restriction digestion as described in the methods.

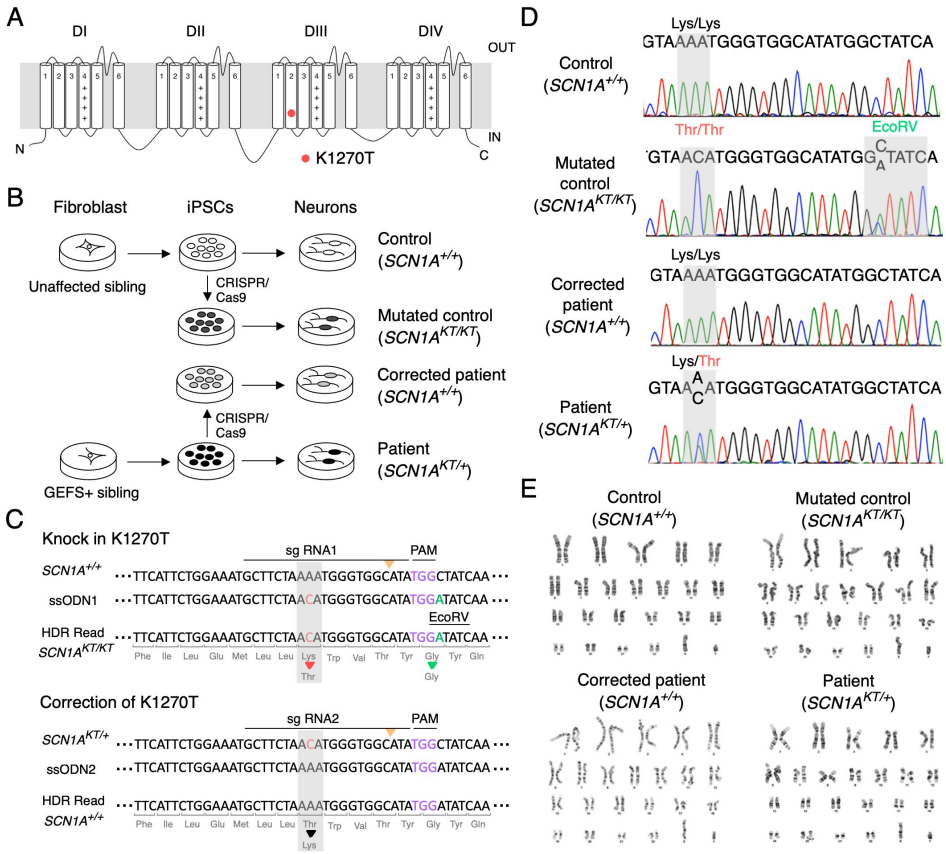

Figure 1. Isogenic pairs of iPSCs generated by CRISPR/Cas9 editing. (A) The K1270T mutation is located at the second transmembrane segment of the third homologous domain of Nav1.1 alpha subunit. (B) CRISPR/Cas9 editing was used to generate two isogenic pairs from iPSCs derived from two siblings in the GEFS+ family (control and patient) followed by differentiation into functional neurons. (C) Scheme of CRISPR/Cas9 editing design. Additional silent mutation introduced by ssODN1 resulted in an EcoRV restriction site for clone screening when knocking in the K1270T mutation. (D) Sequencing of two isogenic iPSC pairs confirmed the absence and the presence of the mutation. (E) All four lines had normal karyotypes (46, XY).

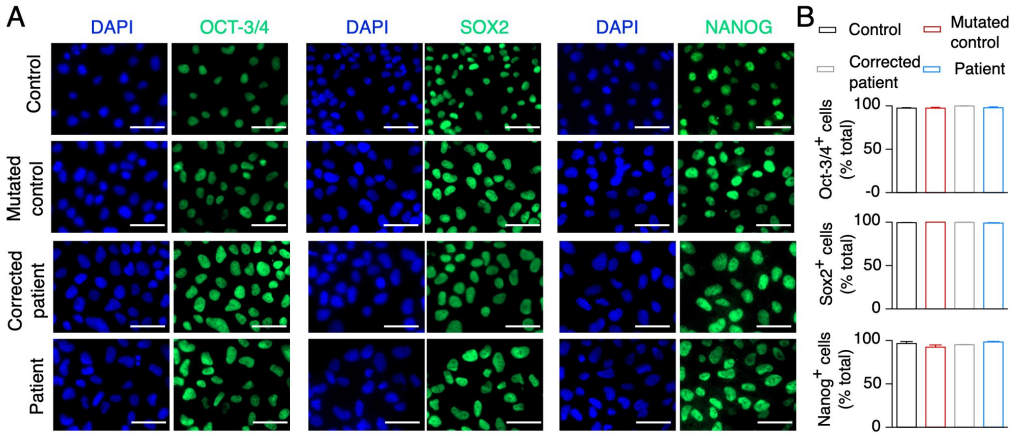

Figure 2. Vast majority of iPSCs in the two isogenic pairs express pluripotency markers. (A) iPSCs of two isogenic pairs were stained with nuclei marker DAPI and pluripotency markers OCT-3/4, SOX2 and NANOG individually. (B) The percentage of cells positive for each of the pluripotency markers. Scale bar represents 50 μm. Data represented as mean + s.e.m. Data represent counts from three fields in three coverslips from three platings for each genotype. Counting was done blind with respect to genotype.

2.2 iPSC-derived neuronal cultures contain both inhibitory and excitatory neurons

We previously optimized a direct differentiation protocol that gives rise to neuronal cultures containing excitatory and inhibitory neurons[32,33]. With this protocol, iPSCs from both isogenic pairs were differentiated into neural progenitors followed by plating onto astroglial feeder layers for neuronal differentiation. To evaluate the morphology of neurons and quantify the proportion of the GABAergic neurons in the cultures derived from the four iPSC lines, cultures were fixed at D21-24 post plating and stained with anti-βIII-tubulin and anti-GABA antibodies. Cultures from all lines contained βIII-tubulin positive cells with elongated branched neurites (Figure 3A). GABAergic neurons comprised 30-40% of the total neuronal population, with no significance between genotypes (Figure 3B).

In order to identify inhibitory and excitatory neurons during live recording, cells were transiently transfected with GAD1-mCherry and CaMKII-eGFP plasmids at D17 post plating. Visualization of the cultures with fluorescent illumination at D21-24 post plating was used to identify and record from mCherry expressing GAD1-positive inhibitory neurons and eGFP expressing

CaMKII-positive excitatory neurons (white arrows, Figure 3C).

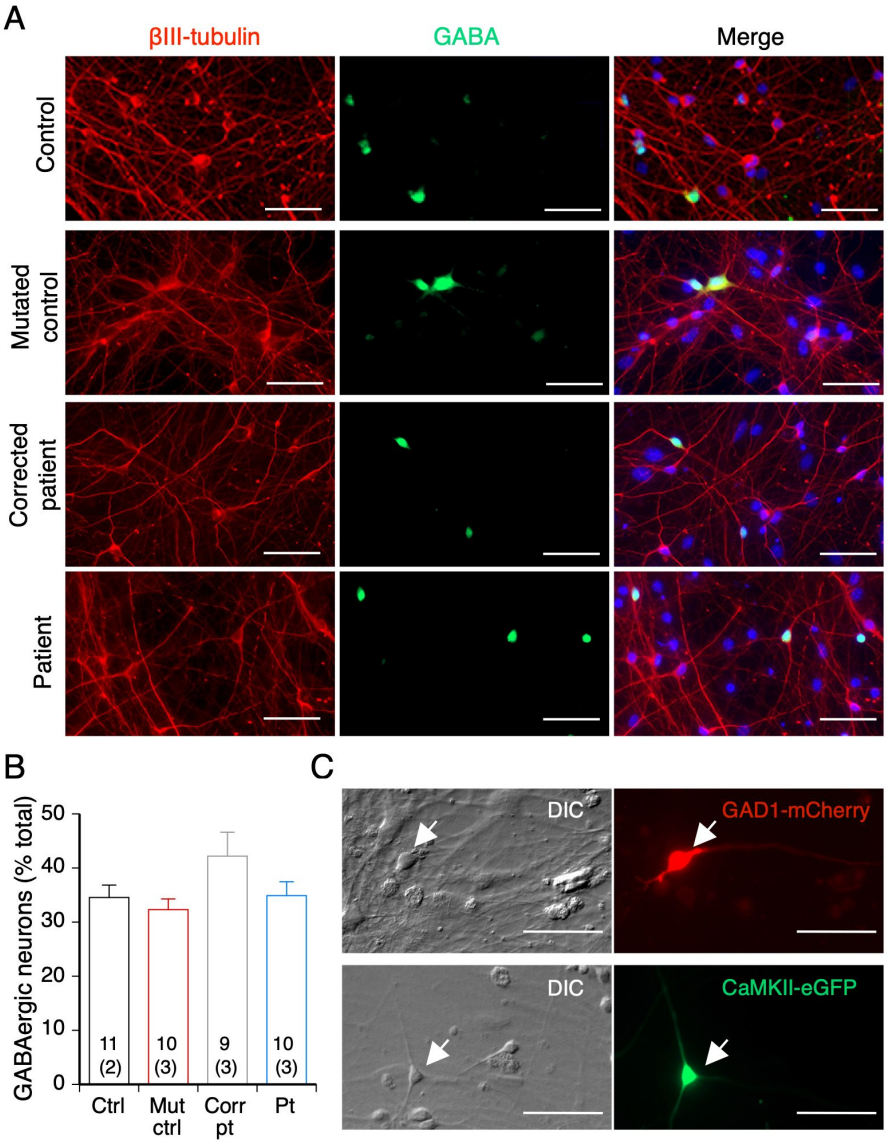

Figure 3. Cultures from two isogenic pairs contain a similar proportion of GABAergic neurons. (A) Representative micrographs from cultures of two isogenic pairs of iPSC-derived neurons stained with nuclei marker DAPI, βIII-tubulin and GABA antibodies to identify GABAergic neurons at D21-24 post plating. (B) The percentage of GABAergic neurons in neuronal cultures at D21-24 post plating in each line. Data represented as mean + s.e.m. Number of coverslips evaluated with number of individual platings shown in parentheses for each line. Ctrl = control, mut ctrl = mutated control, corr pt = corrected patient, and pt = patient. (C) Identification of inhibitory (top) and excitatory (bottom) neurons at D21-24 post plating labeled with transient transfection during live recording (white arrows). Scale bar represents 50 μm.

2.3. Inhibitory neurons: the K1270T mutation reduces sodium current and evoked firing in dose-dependent manner

To determine if the K1270T mutation alters sodium current expression, isolated sodium current recordings were obtained from iPSC-derived inhibitory neurons in cultures from two isogenic pairs: 1a) control (*SCN1A*$^{+/+}$), 1b) mutated control, homozygous (*SCN1A*$^{KT/KT}$); 2a) corrected patient (*SCN1A*$^{+/+}$), 2b) patient, heterozygous (*SCN1A*$^{KT/+}$). To account for variability between platings, and within plating, data for all electrophysiological properties represent recordings from multiple cells in at least three independent platings, and these values are presented in each figure or table.

All inhibitory neurons in each genotype expressed sodium currents at D21-24 post plating. Sodium currents were not well space clamped at this age in culture in any of the lines (Figure 4A and 4C), consistent with the localization of some sodium channels at sites electrically distant from the neuronal cell bodies as is typical of neurons *in vivo*. Therefore, our study focuses on comparing sodium current properties within and between isogenic pairs. While these values may not be reflective of the biophysical properties of sodium currents measured from single channels or in expression systems where there is good voltage control, they allow identification of properties that are or are not associated with the mutation in the native environment.

The mean sodium current density versus voltage curves, generated from analysis of inhibitory neurons in each line of an isogenic pair, were compared. In the mutated control line, homozygous for K1270T, the sodium current density was significantly reduced compared to the control line (interaction: $p = 0.016$, genotype: $p = 0.050$, two-way ANOVA with repeated measures; Figure 4A and 4B). In the patient line, heterozygous for the K1270T mutation, the mean sodium current density versus voltage curve was smaller at each voltage than the corrected line (Figure 4C and 4D). While the difference between the patient and the corrected patient line was not significant, it was about 50% less than that seen between the homozygous mutant and the control line (Figure 4B and 4D). This suggests that the K1270T mutation causes a gene dose-dependent reduction in sodium current density.

No differences were observed in the voltage-dependence of activation, steady-state inactivation, or recovery from inactivation within the isogenic pairs (the mutated control line compared to the control; the patient compared to the corrected patient line; Supplementary Figure 1). However, comparison between the isogenic pairs revealed a ~4 mV depolarized shift in voltage dependence of activation in the pair derived from the control compared to the pair derived from the patient (interaction: $p < 0.0001$, genotype: $p = 0.0065$, two-way ANOVA with repeated measures; Supplementary Figure 1A and 1B and Table 2). There was also a 3 mV depolarized shift in the voltage dependence of steady-state inactivation in the control vs the patient derived lines (interaction: $p < 0.0001$, genotype: $p = 0.2847$, two-way ANOVA with repeated measures; Supplementary Figure 1C and 1D and Table 2). Shifts between pairs are likely associated with the genetic background of the GEFS+ patient.

To determine if the decrease in sodium current density associated with the mutation resulted in a decrease in excitability, the evoked firing properties were examined at D21-D24 post plating. Over 90% of inhibitory neurons in each genotype fired action potentials (Figure 4E and 4G). Assessment of firing frequency vs current step curves in each line demonstrated that the mean firing frequency was significantly lower in the homozygous mutated control line compared to the control line (interaction: $p < 0.0001$, genotype: $p = 0.0092$, two-way ANOVA with repeated measures; Figure 4F). The heterozygous patient line compared to the corrected patient line had decreased firing frequency at small current steps. However, at current steps of 50 pA and above the firing frequency of the patient and the corrected patient line were largely overlapping and the two curves were not significantly different (Figure 4G and 4H). The reduced firing frequency in the heterozygous patient line was approximately half that seen in the homozygous mutated line compared to the control line at the low current steps (Figure 4F and 4H). These data indicate that the impairment of action potential firing in inhibitory neurons, consistent with the changes in sodium current density, is gene dose-dependent.

To evaluate individual AP characteristics, the amplitude and half-width of the first action potential elicited by the rheobase, the injected current that first

elicited AP firing, were compared within the isogenic pairs (Table 3). The AP amplitude was significantly smaller in the homozygous mutated control line compared to the control ($p = 0.0073$, two-tailed unpaired *t* test; Table 3). The AP amplitude was smaller in the heterozygous patient compared to the corrected patient line, approximately half that seen in the first pair, but the difference was not significant (Table 3). This suggests a gene dose-dependent decrease in AP amplitude, consistent with the sodium current and the firing frequency data. There was no significant difference in the AP half-width or the rheobase within or between isogenic pairs (Table 3).

The control and the mutated control had similar input resistance (IR), whole cell capacitance (C_m) and rest membrane potential (RMP; Table 4). Interestingly while the patient line had comparable input resistance to the isogenic corrected line, it had a significantly larger whole cell capacitance and a more hyperpolarized RMP ($p = 0.024$, and < 0.0001 respectively, Mann-Whitney U test for C_m and unpaired *t* test for RMP; Table 4).

Overall the differences within the isogenic pairs demonstrate that the K1270T mutation causes reduced sodium current density, evoked firing, and action potential amplitude in a gene dose-dependent manner in inhibitory neurons. The alterations observed in voltage dependence of activation and steady-state inactivation of sodium currents between isogenic pairs suggest these changes are associated with the genetic background, independent of the mutation.

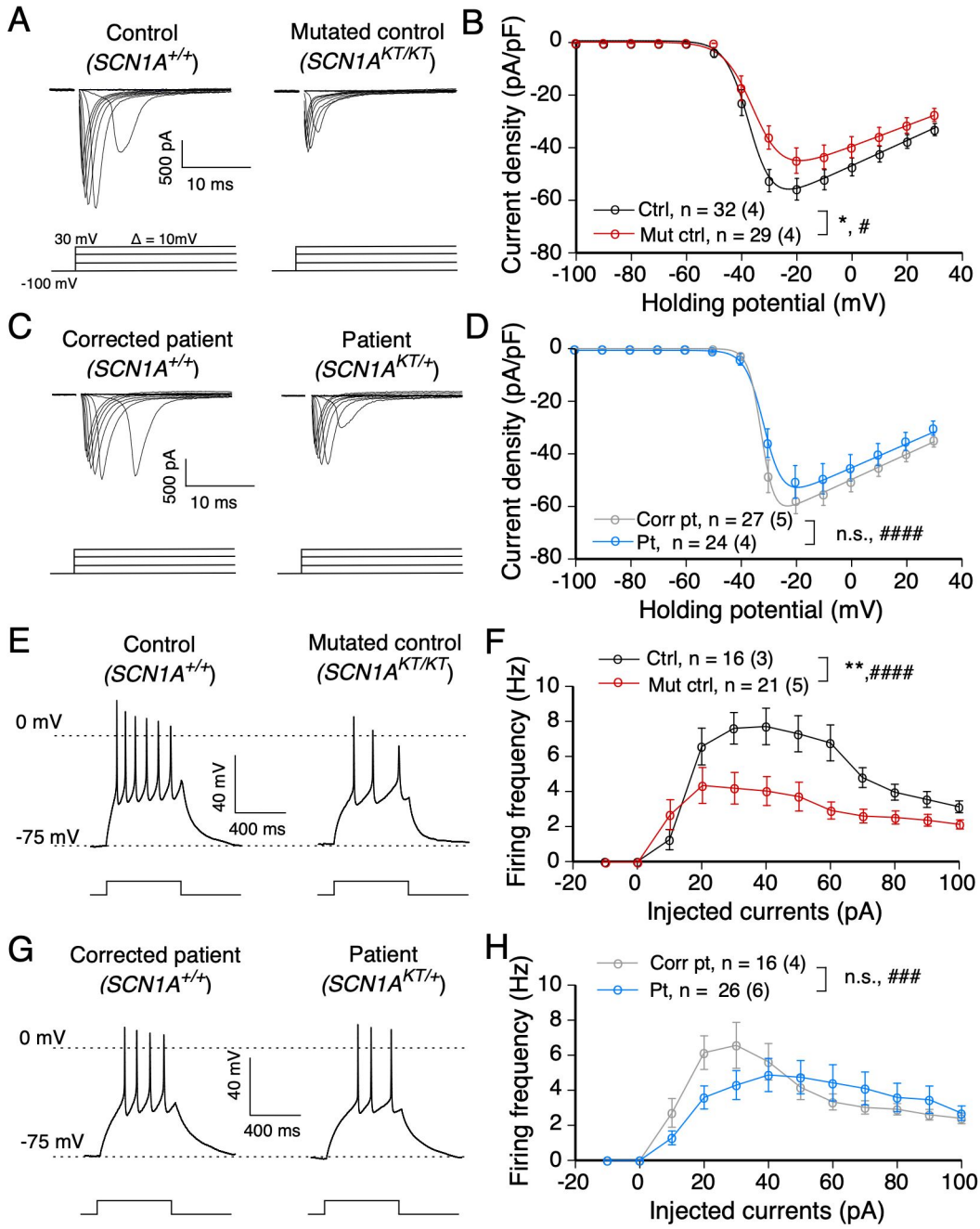

Figure 4. In inhibitory neurons, the K1270T mutation causes reduced sodium current density and impaired AP firing. (A) Representative traces of voltage-gated sodium currents in inhibitory neurons of the first isogenic pair of the control (ctrl) and the homozygous mutated control (mut ctrl). The activation protocol started with a prepulse at -100 mV followed by a series of steps ranging from -100 to 30 mV with a 10 mV interval. (B) Current-voltage relationship in inhibitory neurons of the first isogenic pair. Whole cell currents were normalized to capacitance. (C-D) Same as A and B, but in inhibitory neurons of the second isogenic pair of lines, corrected patient (corr pt) and the heterozygous patient (pt). (E) Representative traces of action potential firing in inhibitory neurons of the first isogenic pair. (F) The input-output curves of action potentials in inhibitory neurons of the first isogenic pair. (G-H) Same as E and F, but in inhibitory neurons of the second isogenic pair. Data presented as mean ± s.e.m with total number of neurons evaluated and the number of individual platings in parentheses for each line. * and # represent significant differences in genotypes and interaction within an isogenic pair respectively, two-way ANOVA and *post hoc* Sidak's analysis. One to four symbols denote p values < 0.05, 0.01, 0.001, 0.0001 respectively.

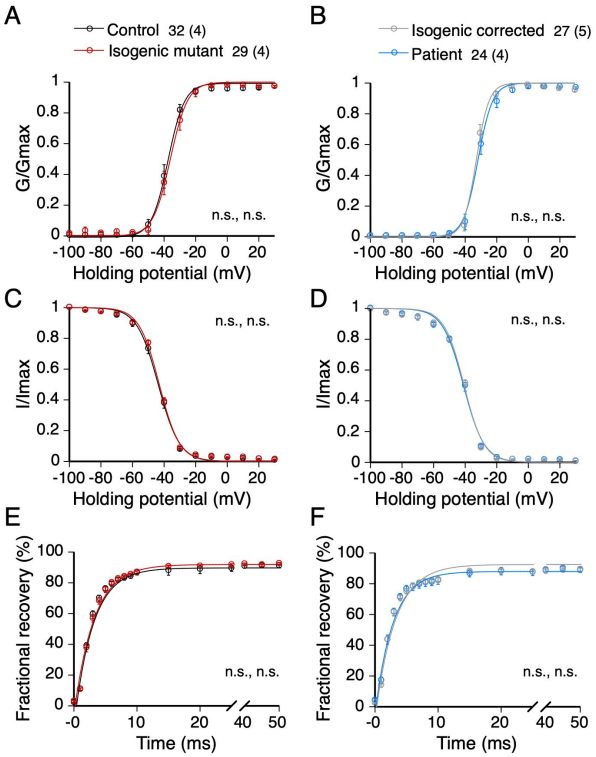

Supplementary Figure 1. Properties of Nav in inhibitory neurons. (A-B) Conductance vs voltage curves of activation in inhibitory neurons of the control vs the mutated control lines, and the corrected patient vs the patient lines respectively. (C-D) Current vs voltage curves of steady-state inactivation in inhibitory neurons of isogenic pairs. (E-F) Recovery of inactivation in both isogenic pairs. Data presented as mean ± s.e.m with total number of neurons and number of individual platings in parentheses evaluated in each line. Two-way ANOVA and *post hoc* Sidak's analysis.

Table 2. Voltage dependence of Nav in isogenic pairs

Cell type	Line	Activation		Inactivation		Recovery
		$V_{1/2}$ (mV)	k (mV)	$V_{1/2}$ (mV)	k (mV)	τ (ms)
Inhibitory	Ctrl, n = 32 (4)	-38.2 ± 1.4	1.7 ± 0.3	-44.0 + 1.0	5.5 ± 0.2	3.0 ± 0.2
	Mut ctrl, n = 29 (4)	-35.1 ± 1.4	2.1 ± 0.3	-43.3 ±0.6	6.3 ± 0.3	3.2 ± 0.2
	Corr pt, n = 27 (5)	-32.0 ± 0.9	2.2 ± 0.3	-41.0 ± 0.4	6.3 ± 0.3	2.8 ± 0.1
	Pt, n =24 (4)	-31.3 ± 1.3	2.5 ± 0.4	-41.0 ± 0.8	6.1 ± 0.3	2.9 ± 0.2
Excitatory	Ctrl, n = 36 (4)	-35.4 ± 1.1	1.7 ± 0.2	-43.2 ± 0.5	5.7 ± 0.1	3.0 ± 0.1
	Mut ctrl, n = 27 (4)	-35.3 ± 1.3	2.2 ± 0.3	-44.0 ± 0.9	5.8 ± 0.2	3.4 ± 0.2
	Corr pt, n = 26 (5)	-31.5 ± 1.0*	2.3 ± 0.3	-42.5 ± 0.7*	7.2 ± 0.5**	2.9 ± 0.1
	Pt, n = 26 (4)	-34.7 ± 1.0	2.0 ± 0.3	-40.5 ± 0.4	5.4 ± 0.2	3.1 ± 0.1

Data reported as mean ± s.e.m with total number of neurons and number of individual platings in parentheses for each line. Ctrl = control, mut ctrl = mutated control, corr pt = corrected patient, and pt = patient. Statistically significant differences within isogenic pairs: * $p < 0.05$ and *** $p < 0.001$, two-tailed unpaired *t*-test for activation and inactivation $V_{1/2}$, and Mann-Whitney U test for inactivation k.

Table 3. Measurements of excitability in two isogenic pairs

Cell type	Genotype	Rheobase (pA)	AP amplitude (mV)	AP half-width (ms)
Inhibitory	Ctrl	18.8 ± 1.7 n = 13 (3)	58.5 ±1.8 n = 16 (3)	3.6 ± 0.2 n = 16 (3)
	Mut ctrl	22.5 ± 3.8 n = 16 (5)	45.6 ± 3.8 ** n = 19 (5)	4.8 ±0.6 n = 19 (5)
	Corr pt	15.3 ± 1.7 n = 15 (4)	47.5 ± 3.4 n = 16 (4)	4.6 ± 0.7 n = 16 (4)
	Pt	23.9 ± 3.3 n = 26 (6)	41.1 ± 2.9 n = 25 (6)	6.1 ± 0.8 n = 25 (6)
Excitatory	Ctrl	23.3 ± 2.4 n = 9 (3)	57.2 ± 2.8 n = 15 (3)	3.9 ± 0.4 n = 15 (3)
	Mut ctrl	21.3 ± 1.9 n = 15 (5)	55.7 ± 1.6 n = 29 (5)	3.9 ± 0.2 n = 29 (5)
	Corr pt	17.5 ± 1.9 n = 16 (5)	55.1 ± 2.5 n = 16 (5)	4.0 ± 0.5 n = 16 (5)
	Pt	18.7 ± 2.4 n = 32 (8)	57.0 ± 1.8 n = 33 (8)	4.2 ± 0.2 n = 33 (8)

Data reported as mean ± s.e.m with total number of neurons (number of individual platings) underneath. Ctrl = control, mut ctrl = mutated control, corr pt = corrected patient, and pt = patient. Statistically significant differences within isogenic pairs: ** $p < 0.01$, two-tailed unpaired *t*-test.

Table 4. Passive membrane properties in two isogenic pairs

Cell type	Genotype	IR (GΩ)	C_m (pF)	RMP (mV)
Inhibitory	Ctrl	1.6 ± 0.1 n = 16 (3)	27.3 ± 2.8 n = 15 (3)	-43.0 ± 2.7 n = 13 (3)
	Mut ctrl	1.6 ± 0.1 n = 21 (5)	27.8 ± 2.8 n = 22 (5)	-44.3 ± 2.7 n = 18 (5)
	Corr pt	1.6 ± 0.2 n = 22 (4)	32.1 ± 2.4* n = 22 (4)	-57.8 ± 1.3**** n = 17 (2)
	Pt	1.6 ± 0.1 n = 26 (6)	24.9 ± 2.3 n = 26 (6)	-45.8 ± 2.3 n = 13 (2)
Excitatory	Ctrl	1.0 ± 0.1 n = 16 (3)	30.5 ± 2.5 n = 15 (3)	-47.0 ± 0.3 n = 9 (3)
	Mut ctrl	1.3 ± 0.09* n = 30 (5)	32.6 ± 2.9 n = 28 (5)	-44.9 ± 2.3 n = 17 (5)
	Corr pt	1.3 ± 0.09 n = 24 (5)	31.3 ± 1.4 n = 24 (5)	-51.1 ± 2.0 n = 14 (2)
	Pt	1.5 ± 0.09 n = 48 (8)	36.7 ± 1.8 n = 48 (8)	-49.1 ± 2.4 n = 12 (2)

Data reported as mean ± s.e.m with total number of neurons and number of individual platings in parentheses. Ctrl = control, mut ctrl = mutated control, corr pt = corrected patient, and pt = patient. Statistically significant differences within isogenic pair: * $p < 0.05$ and **** $p < 0.0001$, two-tailed Mann-Whitney U test for IR and C_m and unpaired *t*-test for RMP.

2.4. Excitatory neurons: the K1270T mutation causes a reduction in sodium

current density, but does not impair evoked firing

Previous studies in mouse models have suggested that *SCN1A* mutations alter sodium currents specifically in inhibitory neurons. However, a study using iPSC lines showed both excitatory and inhibitory neurons are affected by an *SCN1A* mutation [23]. To determine if this was true in our system, isolated sodium current recordings were obtained from iPSC-derived excitatory neurons for each of the 4 genotypes in the same two isogenic pairs examined in the previous section. Similar to inhibitory neurons, all cells expressed sodium currents that were not well clamped (Figure 5A and 5C).

The current density vs voltage curve demonstrated a significant reduction in sodium current density in the homozygous mutated control line compared to the control line (interaction: $p < 0.0001$, genotype: $p = 0.0025$, two-way ANOVA with repeated measures; Figure 5B). The decrease in sodium current density in the heterozygous patient line compared to the corrected patient line was also significant (interaction: $p < 0.0001$, genotype: $p = 0.056$, two-way ANOVA with repeated measures; Figure 5D) and approximately half the magnitude seen in the homozygous mutated control line (Figure 5B and 5D). This is consistent with the dose-dependent reduction in sodium current observed in the inhibitory neurons.

The voltage dependence of activation and steady-state inactivation in the homozygous mutated control was not different than the control (Table 2 and Supplementary Figure 2A and 2C). In contrast, there was a hyperpolarized shift in the voltage-dependence of activation and a depolarized shift in steady-state inactivation in the heterozygous patient compared to the corrected patient line ($p = 0.028$ and 0.015 respectively, two-tailed unpaired *t* test; Table 2 and Supplementary Figure 2B and 2D). This indicates that the differences in activation and steady-state inactivation in the second isogenic pair result from an interaction between the K1270T mutation and the patient genetic background. All the lines recovered from inactivation with a similar time constant of ~3 ms (Table 2 and Supplementary Figure 2E and 2F).

Since the mutation resulted in a reduction of sodium current density in excitatory neurons, the firing properties were examined in each of the 4

genotypes at D21-24 post plating. Over 93% of excitatory neurons in each genotype fired action potentials with injection of depolarizing currents (Figure 5E and 5G). However, in contrast to expectations based on reduced sodium current expression, the firing frequency versus current step curves demonstrated the firing frequency in the homozygous mutated control was not different from the control (Figure 5F). A similar or higher firing frequency was also observed in the heterozygous patient line compared to the corrected patient line (interaction: $p = 0.0042$, genotype: $p = 0.041$, two-way ANOVA with repeated measures; Figure 5H). There was no significant difference in the rheobase, firing frequency, AP amplitude and AP half-width within or between the isogenic pair (Table 3).

The input resistance in the mutated control was slightly higher than that of the control ($p = 0.025$, two-tailed Mann-Whitney U test; Table 4). However there was no difference in the input resistance between the patient vs the corrected patient line (Table 4). The whole cell capacitance and RMP were similar within the isogenic pairs (Table 4).

Taken together, similar to the inhibitory neurons, the K1270T mutation causes reduced sodium current density in excitatory neurons in a dose-dependent manner. However, the decreased sodium current density caused by the mutation in excitatory neurons is not sufficient to alter the evoked firing or AP waveforms. The alterations in the voltage dependence of activation and inactivation of sodium currents only in the patient derived isogenic pair but not the control derived isogenic pair, indicate these changes are dependent on an interaction between the mutation and the patient genetic background.

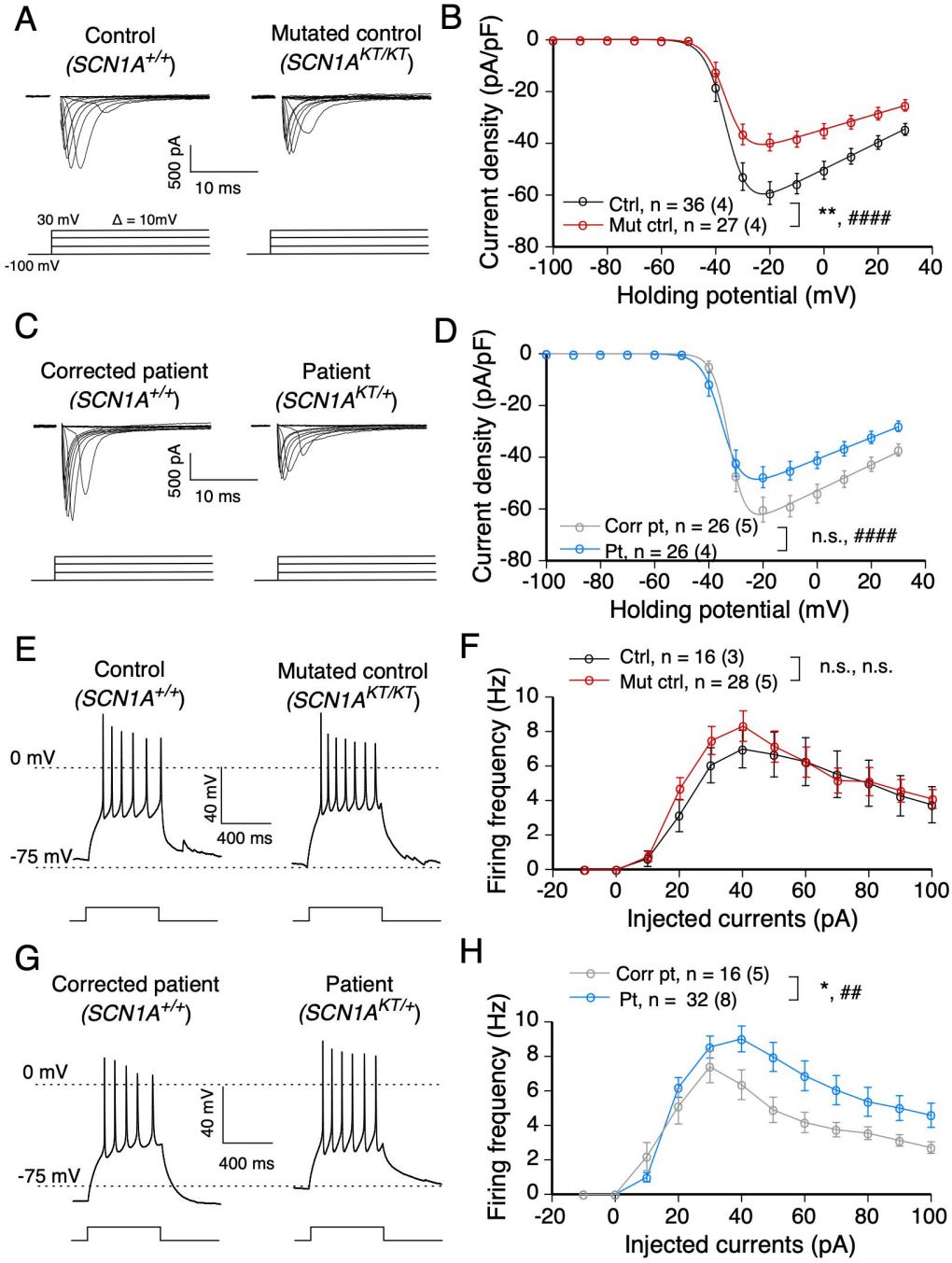

Figure 5. In excitatory neurons, the K1270T mutation gives rise to decreased sodium current density but does not affect AP firing. (A) Representative traces of voltage-gated sodium currents in inhibitory neurons of the first isogenic pair of the control (ctrl) and the homozygous mutated control (mut ctrl) lines. The activation protocol started with a prepulse at -100 mV followed by a series of steps ranging from -100 to 30 mV with a 10 mV interval. (B) Current-voltage relationship in inhibitory neurons of the first isogenic pair. Whole cell currents were normalized to capacitance. (C-D) Same as A and B, but in inhibitory neurons of the second isogenic pair of the corrected patient (corr pt) and the heterozygous patient (pt) lines. (E) Representative traces of action potential firing in inhibitory neurons of the first isogenic pair. (F) The input-output curves of action potentials in inhibitory neurons of the first isogenic pair. (G-H) Same as E and F, but in inhibitory neurons of the second isogenic pair. Data presented as mean ± s.e.m with total number of neurons and number of individual platings in parentheses. * and # represent significant differences in genotypes and interaction within an isogenic pair respectively, two-way ANOVA and *post hoc* Sidak's analysis. One to four symbols denote p values < 0.05, 0.01, 0.001, 0.0001 respectively.

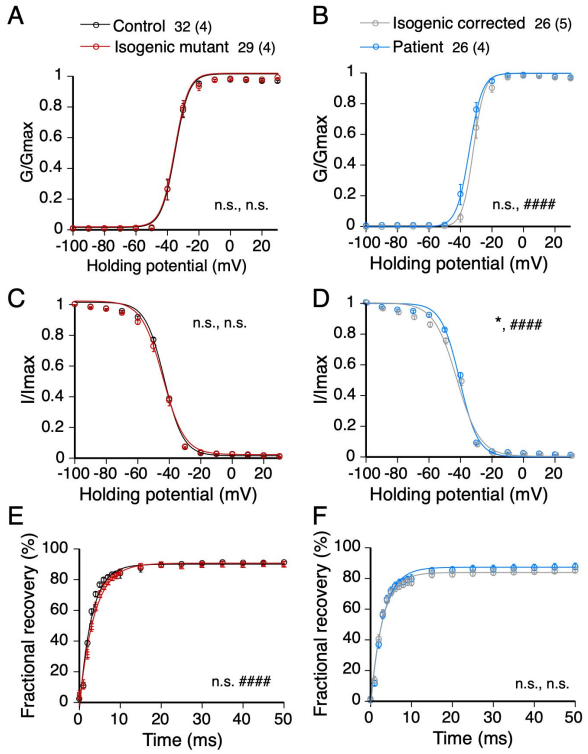

Supplementary Figure 2. Properties of Nav in excitatory neurons. (A-B) Conductance vs voltage curves of activation in excitatory neurons of the control vs the mutated control lines, and the corrected patient vs the patient lines respectively. (C-D) Current vs voltage curves of steady-state inactivation in excitatory neurons of isogenic pairs. (E-F) Recovery of inactivation in both isogenic pairs. Data presented as mean ± s.e.m with total number of neurons and number of individual platings in parentheses. * and # represent significant differences in genotypes and interaction within an isogenic pair respectively, two-way ANOVA and *post hoc* Sidak's analysis. One and four symbols denote p values < 0.05, and 0.0001 respectively.

2.5. The K1270T mutation results in a hyperexcitable network.

A previous study from our laboratory found that the large majority of neurons in iPSC-derived cultures receive spontaneous glutamatergic and GABAergic synaptic input at D21-24 post plating[32]. To determine if the K1270T mutation, that specifically reduces firing of inhibitory neurons, causes an increase in excitability of the neuronal network, spontaneous excitatory and inhibitory post-synaptic currents (sEPSCs and sIPSCs) were recorded from excitatory neurons in each genotype.

All neurons that received both sEPSCs and sIPSCs were included for analysis. Recordings were obtained at two different holding potentials, -2 mV and -49 mV in each neuron corresponding to the reversal potential for EPSCs and IPSCs, respectively (Figure 6A and 6D). To determine whether there was any change in the balance of excitation vs inhibition, an index, (E-I)/(E+I) was used, where E and I represented amplitude or charge transfer of sEPSC and sIPSC respectively in excitatory neurons. This symmetric index ensures that E and I have the same scale, in contrast of the ratio of E/I. An increase in the (E-I)/(E+I) index would indicate an increase in excitatory drive or a decrease in inhibitory drive, and vice versa.

The (E-I)/(E+I) index based both on synaptic current amplitude and charge transfer, was significantly larger ($p = 0.0002$ and 0.0464 respectively, two-tailed Mann-Whitney U test) in the homozygous mutated control line compared to the control and these differences were significant ($p = 0.0002$ and 0.0464 respectively, two-tailed Mann-Whitney test; Figure 6B and 6C). In contrast, the data showed a trend of larger (E-I)/(E+I) index in the heterozygous patient line compared to the corrected patient line. However, these differences were not significant (Figure 6E and 6F). This indicates the mutation results in a dose-dependent increase of excitability in the neural networks formed in these cultures, consistent with the effects of mutation on sodium currents and evoked firing in inhibitory neurons.

To test whether the increased excitatory drive in the network was also influenced by alterations in synaptic vesicle release, miniature excitatory and inhibitory PSCs (mEPSCs and mIPSCs) were recorded in excitatory neurons in the presence of 1 μM tetrodotoxin to block action potentials. The frequency, amplitude, and charge transfer of mEPSCs were similar between genotypes with the same genetic background (Supplementary Figure 3A-C). There were also no changes in the mIPSCs (Supplementary Figure 3D-F). This suggests that the K1270T mutation does not affect the synaptic vesicle release.

Together these data indicate that the K1270T mutation results in a dosage-dependent imbalance in excitation and inhibition that leads to hyperactivity in the neural network.

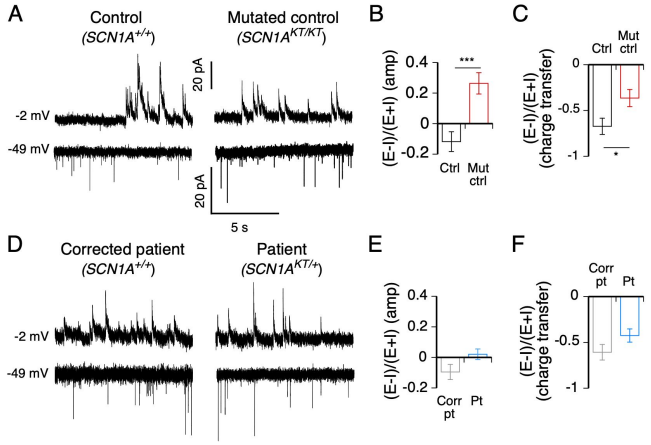

Figure 6. The K1270T mutation gives rise to a hyperactive neural network. (A) Spontaneous excitatory and inhibitory post-synaptic currents received by excitatory neurons in the first isogenic pair of the control (ctrl) and the mutated control (mut ctrl) line. (B) The ratio of spontaneous (E-I)/(E+I) amplitude in excitatory neurons of the first isogenic pair. (C) The ratio of spontaneous (E-I)/(E+I) of charge transfer in excitatory neurons of the first isogenic pair. (D-F) Same as A-C, but in excitatory neurons of the second isogenic pair of the corrected patient (corr pt) and the patient (pt) lines. Data reported as mean ± s.e.m. The total number of neurons and number of platings in parentheses for all four lines are 29 (7), 17 (4), 13 (3), and 18 (3) respectively. *$p < 0.05$ and ***$p < 0.0001$, two-tailed Mann-Whitney U test.

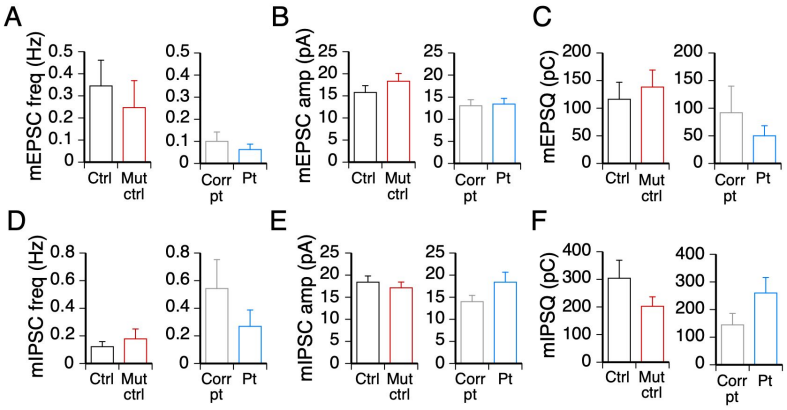

Supplementary figure 3. Miniature EPSCs IPSCs received by excitatory neurons were unaltered by the K1270T mutation. (A-C) The frequency, amplitude and charge transfer of mEPSCs in the control (ctrl) vs the mutated control (mut ctrl), and the corrected patient (corr pt) vs the patient (pt) lines. (D-F) Same as A-C, but for mIPSCs. Data reported as mean + s.e.m. The total number of neurons and number of individual platings in parentheses for all four lines are ctrl: 9 (5), mut ctrl: 7 (3), corr pt:10 (4), and pt:10 (3).

3. Discussion

3.1 Neuronal subtype-specific alterations in sodium current density and excitability

Our results demonstrate that in inhibitory neurons, the K1270T *SCN1A* mutation causes dosage-dependent decrease in sodium current density and evoked firing. Whereas previous studies have reported mutation of *SCN1A* has little effect on sodium currents in excitatory neurons[21,35,36], here we show that the K1270T mutation has no effect on evoked firing of excitatory neurons but does produce a dose-dependent decrease in sodium current density. Although the dominant Nav isoform in excitatory neurons is Nav1.6[38], it has been reported that Nav1.1 is also present in a subset of excitatory neurons[39,40]. Together with the evidence from the induction and rescue of reduced sodium current density in the isogenic lines, the results suggest alterations in sodium currents in excitatory neurons are associated with the mutation. However, in our study the evoked firing rate in excitatory neurons was unaltered or slightly increased in the mutated control and patient lines respectively, indicating that the changes in the sodium current density were not sufficient to influence the excitability of the cells. It could be due to compensation from potassium currents, as a voltage-gated potassium channel Kv8.2 has been shown to function as a genetic modifier increasing the susceptibility of an *Scn2a* mutant mouse to epilepsy[41,42]. Altered currents of Kv1 and Kv4 are associated with increased excitability in a subset of pyramidal neurons in a mouse model of fragile X syndrome[43]. *CACNB4* and *CACNA1A* that encode Cav have also been identified as genetic modifiers that result in a gain of function in families with *SCN1A* Dravet syndrome[44,45]

The dosage-dependent effect of the K1270T mutation is similar to the observations of sodium currents and evoked firing rate of bipolar cells that were selectively affected in the mouse model of Dravet Syndrome (DS) with partial deletion of *Scn1a*[36]. In another mouse model with GEFS+ *SCN1A* R1648H mutation, although dosage-dependent cellular effects were not observed, the homozygous mice had a higher susceptibility to seizures than the heterozygous mice in comparison to the wild types[35]. Therefore, our study is consistent with

the findings *in vivo* and predicts a functional outcome of the K1270T mutation on the seizure generation in animal models.

3.2 Alterations that are not associated with the mutation in the patient line

Although the mutated control line in our study recapitulates most of the defects in the patient line, there are alterations in the Nav function that are not associated with the K1270T mutation that were observed in both the patient and the corrected patient lines. These defects include the depolarized shift in the voltage dependence of inactivation in both neuronal subtypes and the depolarized shift of activation in inhibitory neurons. Since the genetic analysis in the original case study for the K1270T mutation was performed in the whole family, identification of *de novo SCN1A* mutations that has been reported in individual GEFS+ patients would provide insight into individual phenotypic differences[14,46]. It is also likely that genetic background harbors genetic modifiers that exacerbate or ameliorate the cellular defects. For instance, a missense mutation in *SCN9A* that encodes Nav1.7 has been identified in *SCN1A*-associated epilepsy patients[47]. To identify genetic modifiers that are altered in the *SCN1A* GEFS+ mutants, single cell RNA sequencing will be useful for screening candidates in a high-throughput manner[48].

3.3 Comparison with the previous knock-in fly model

The reduced excitability observed specifically in iPSC-derived inhibitory neurons is consistent with the decreased excitability specifically in inhibitory neurons in the brains of K1270T GEFS+ knock-in *Drosophila*[49]. Since both flies and patients exhibit heat-induced seizures, this provides additional support to the hypothesis that reduced firing specifically in inhibitory neurons is critical to the disease phenotype in humans. However, the cellular defect associated with reduced excitability is distinct between the models demonstrating two independent mechanisms that result in a similar phenotype. In the iPSC-derived neurons there is a significant decrease in the amplitude of the transient currents that are the dominant form of sodium current in these neurons. In flies the reduced firing is associated with a hyperpolarized shift in the deactivation

threshold of the large persistent sodium currents characteristic of inhibitory neurons in the adult fly brain. It is possible that modifying the persistent current in iPSCs by shifting their voltage dependence could moderate the deficits associated with a reduced transient sodium current. In addition, the alterations in fly are seen predominantly at high temperature so it is possible that elevated temperatures will reveal additional or more severe alterations in sodium currents in iPSC-derived neurons.

3.4 Advantages of dual isogenic pair approach

Dual isogenic pairs, that include patient-derived iPSCs and the corrected line, as well as control-derived iPSCs into which the disease-associated mutation has been introduced have significant advantages. Alterations that are seen in both mutant lines and not in the control or corrected lines, identify mutations that are not only necessary but sufficient to cause the genotype[29,50,51] as is the case in the present study with changes in sodium currents and firing properties. This strategy also allows for identification of alterations due to the genetic background based on changes that are found in both lines of one isogenic pair but not in the other isogenic pair[29], as is seen in the voltage dependence of Nav activation and inactivation in inhibitory neurons of the patient-derived pair only. Further, a change in one mutant line that is not seen in the other mutant line, identifies alterations associated with an interaction between the mutation and the genetic background, as is observed in the voltage dependence of Nav activation and inactivation in excitatory neurons of the patient line.

Overall the CRISPR/Cas9-based disease modeling strategy with iPSC-derived neurons can validate clinically relevant phenotypes and reveal the sufficiency and necessity of *SCN1A* mutations for specific phenotypes in the human genetic background. Furthermore, a library of patient iPSCs with a variety of *SCN1A* mutations built using this approach, in combination with a high-throughput drug screening method such as multi-electrode array (MEA), will facilitate the development of personalized anti-epileptic medicine[52–54].

4. Acknowledgement

This work was supported by the National Institutes of Health grants R01 NS083009 (D.K.O.), R01 GHD059967 grant (P.H.S.), and R01 NS078289 (K.C.E.) and a California Institute for Regenerative Medicine Bridges to Stem Cell Research grant CIRM-EDUC2-08383 (C.M.R.). We would also like to thank Alexander E. Stover for generating the iPSCs, Priscilla Figueroa, Noor Osman and Daniel R. Benavides for help on astroglial cultures, Sara E. Konopelski for help on screening of clones, Karla Soto Sauza for help on immunostaining and cell counting and Longwen Huang for input on the manuscript.

5. Author contributions

The laboratory of K.C.E. provided skin fibroblasts from the unaffected sibling and the patient sibling from the GEFS+ family. The laboratory of P.H.S. reprogrammed the fibroblasts into iPSCs. O.S.S. and M.A.S. designed the CRISPR/Cas9, and O.S.S., Y.X., N.N.N. and C.M.R. performed screening of positive clones. C.M.R., N.N.N., O.S.S. and Y.X. prepared astroglial cultures. Y.X., N.N.N. and C.M.R differentiated iPSCs into neurons. Y.X. and N.N.N. performed electrophysiological recording. Y.X., N.N.N. and C.M.R analyzed the electrophysiology data. Y.X. and N.N.N. performed immunostaining, imaging and cell counting. Y.X. wrote the manuscript, N.N.N., O.S.S., K.C.E, P.H.S., M.A.S. and D.K.O. edited the manuscript.

References

1. Scheffer, I. E. & Berkovic, S. F. Generalized epilepsy with febrile seizures plus. A genetic disorder with heterogeneous clinical phenotypes. *Brain* **120,** 479–490 (1997).
2. Miller, I. & Sotero de Menezes, M. *SCN1A-Related Seizure Disorders*. (University of Washington, Seattle, 2014).
3. Escayg, A. *et al.* Mutations of SCN1A, encoding a neuronal sodium channel, in two families with GEFS+2. *Nat. Genet.* **24,** 343–345 (2000).
4. Escayg, A. *et al.* A novel SCN1A mutation associated with generalized

epilepsy with febrile seizures plus--and prevalence of variants in patients with epilepsy. *Am. J. Hum. Genet.* **68,** 866–873 (2001).

5. Sugawara, T. *et al.* A missense mutation of the Na+ channel alpha II subunit gene Na(v)1.2 in a patient with febrile and afebrile seizures causes channel dysfunction. *Proc. Natl. Acad. Sci. U. S. A.* **98,** 6384–6389 (2001).
6. Harkin, L. A. *et al.* Truncation of the GABA(A)-receptor gamma2 subunit in a family with generalized epilepsy with febrile seizures plus. *Am. J. Hum. Genet.* **70,** 530–536 (2002).
7. Wallace, R. H. *et al.* Febrile seizures and generalized epilepsy associated with a mutation in the Na+-channel beta1 subunit gene SCN1B. *Nat. Genet.* **19,** 366–370 (1998).
8. Wallace, R. H. *et al.* Generalized epilepsy with febrile seizures plus: mutation of the sodium channel subunit SCN1B. *Neurology* **58,** 1426–1429 (2002).
9. Baulac, S. *et al.* First genetic evidence of GABA(A) receptor dysfunction in epilepsy: a mutation in the gamma2-subunit gene. *Nat. Genet.* **28,** 46–48 (2001).
10. Wallace, R. H. *et al.* Mutant GABA(A) receptor gamma2-subunit in childhood absence epilepsy and febrile seizures. *Nat. Genet.* **28,** 49–52 (2001).
11. Dibbens, L. M. *et al.* GABRD encoding a protein for extra- or peri-synaptic GABAA receptors is a susceptibility locus for generalized epilepsies. *Hum. Mol. Genet.* **13,** 1315–1319 (2004).
12. Wallace, R. H. *et al.* Neuronal sodium-channel alpha1-subunit mutations in generalized epilepsy with febrile seizures plus. *Am. J. Hum. Genet.* **68,** 859–865 (2001).
13. Meng, H. *et al.* The SCN1A mutation database: updating information and analysis of the relationships among genotype, functional alteration, and phenotype. *Hum. Mutat.* **36,** 573–580 (2015).
14. Abou-Khalil, B. *et al.* Partial and generalized epilepsy with febrile seizures plus and a novel SCN1A mutation. *Neurology* **57,** 2265–2272 (2001).

15. Goldberg-Stern, H. *et al.* Broad phenotypic heterogeneity due to a novel SCN1A mutation in a family with genetic epilepsy with febrile seizures plus. *J. Child Neurol.* **29,** 221–226 (2014).
16. Schutte, S. S., Schutte, R. J., Barragan, E. V & O'Dowd, D. K. Model systems for studying cellular mechanisms of SCN1A-related epilepsy. *J. Neurophysiol.* **115,** 1755–1766 (2016).
17. Marian, A. J. Modeling human disease phenotype in model organisms: 'It's only a model!' *Circ. Res.* **109,** 356–359 (2011).
18. Maxwell, E. K. *et al.* Evolutionary profiling reveals the heterogeneous origins of classes of human disease genes: implications for modeling disease genetics in animals. *BMC Evol. Biol.* **14,** 212 (2014).
19. Higurashi, N. *et al.* A human Dravet syndrome model from patient induced pluripotent stem cells. *Mol. Brain* **6,** 19 (2013).
20. Liu, J. *et al.* CRISPR/Cas9 facilitates investigation of neural circuit disease using human iPSCs: mechanism of epilepsy caused by an SCN1A loss-of-function mutation. *Transl Psychiatry* **6,** e703 (2016).
21. Sun, Y. *et al.* A deleterious Nav1.1 mutation selectively impairs telencephalic inhibitory neurons derived from Dravet Syndrome patients. *Elife* **5,** e13073 (2016).
22. Jiao, J. *et al.* Modeling Dravet syndrome using induced pluripotent stem cells (iPSCs) and directly converted neurons. *Hum. Mol. Genet.* **22,** 4241–4252 (2013).
23. Liu, Y. *et al.* Dravet syndrome patient-derived neurons suggest a novel epilepsy mechanism. *Ann. Neurol.* **74,** 128–139 (2013).
24. Vitale, A. M. *et al.* Variability in the Generation of Induced Pluripotent Stem Cells: Importance for Disease Modeling. *Stem Cells Translational Medicine* **1,** 641–650 (2012).
25. Liang, G. & Zhang, Y. Genetic and epigenetic variations in iPSCs: potential causes and implications for application. *Cell stem cell* **13,** 149–159 (2013).
26. Sandoe, J. & Eggan, K. Opportunities and challenges of pluripotent stem cell neurodegenerative disease models. *Nat Neurosci* **16,** 780–789

(2013).

27. Chen, W. *et al.* Generation of the SCN1A epilepsy mutation in hiPS cells using the TALEN technique. *Sci. Rep.* **4,** 5404 (2014).
28. Bassett, A. R. Editing the genome of hiPSC with CRISPR/Cas9: disease models. *Mamm. Genome* **28,** 348–364 (2017).
29. Smith, J. G. W. *et al.* Isogenic Pairs of hiPSC-CMs with Hypertrophic Cardiomyopathy/LVNC-Associated ACTC1 E99K Mutation Unveil Differential Functional Deficits. *Stem cell reports* **11,** 1226–1243 (2018).
30. Stover, A. E. *et al.* Process-based expansion and neural differentiation of human pluripotent stem cells for transplantation and disease modeling. *J. Neurosci. Res.* **91,** 1247–1262 (2013).
31. Stover, A. E. & Schwartz, P. H. Adaptation of Human Pluripotent Stem Cells to Feeder-Free Conditions in Chemically Defined Medium with Enzymatic Single-Cell Passaging. *Methods Mol. Biol.* **767,** 137–146 (2011).
32. Xie, Y. *et al.* Reproducible and efficient generation of functionally active neurons from human hiPSCs for preclinical disease modeling. *Stem Cell Res.* **26,** 84–94 (2018).
33. Schutte, R. J. *et al.* Astrocyte-enriched feeder layers from cryopreserved cells support differentiation of spontaneously active networks of human iPSC-derived neurons. *J. Neurosci. Methods* **294,** 91–101 (2018).
34. Paquet, D. *et al.* Efficient introduction of specific homozygous and heterozygous mutations using CRISPR/Cas9. *Nature* **533,** 125–129 (2016).
35. Martin, M. S. *et al.* Altered function of the SCN1A voltage-gated sodium channel leads to gamma-aminobutyric acid-ergic (GABAergic) interneuron abnormalities. *J. Biol. Chem.* **285,** 9823–9834 (2010).
36. Yu, F. H. *et al.* Reduced sodium current in GABAergic interneurons in a mouse model of severe myoclonic epilepsy in infancy. *Nat. Neurosci.* **9,** 1142–1149 (2006).
37. Yu, J. *et al.* Induced pluripotent stem cell lines derived from human somatic cells. *Science* **318,** 1917–1920 (2007).

38. Lorincz, A. & Nusser, Z. Cell-type-dependent molecular composition of the axon initial segment. *J. Neurosci.* **28,** 14329–14340 (2008).
39. Dutton, S. B. *et al.* Preferential inactivation of Scn1a in parvalbumin interneurons increases seizure susceptibility. *Neurobiol. Dis.* **49,** 211–220 (2013).
40. Ogiwara, I. *et al.* Nav1.1 haploinsufficiency in excitatory neurons ameliorates seizure-associated sudden death in a mouse model of Dravet syndrome. *Hum. Mol. Genet.* **22,** 4784–4804 (2013).
41. Bergren, S. K., Rutter, E. D. & Kearney, J. A. Fine mapping of an epilepsy modifier gene on mouse Chromosome 19. *Mamm. Genome* **20,** 359–366 (2009).
42. Jorge, B. S. *et al.* Voltage-gated potassium channel KCNV2 (Kv8.2) contributes to epilepsy susceptibility. *Proc. Natl. Acad. Sci.* **108,** 5443 LP-5448 (2011).
43. Kalmbach, B. E., Johnston, D. & Brager, D. H. Cell-Type Specific Channelopathies in the Prefrontal Cortex of the fmr1-/y Mouse Model of Fragile X Syndrome. *eNeuro* **2,** ENEURO.0114-15.2015 (2015).
44. Ohmori, I. *et al.* A CACNB4 mutation shows that altered Ca(v)2.1 function may be a genetic modifier of severe myoclonic epilepsy in infancy. *Neurobiol. Dis.* **32,** 349–354 (2008).
45. Ohmori, I. *et al.* CACNA1A variants may modify the epileptic phenotype of Dravet syndrome. *Neurobiol. Dis.* **50,** 209–217 (2013).
46. Myers, K. A. *et al.* De novo SCN1A pathogenic variants in the GEFS+ spectrum: Not always a familial syndrome. *Epilepsia* **58,** e26–e30 (2017).
47. Singh, N. A. *et al.* A role of SCN9A in human epilepsies, as a cause of febrile seizures and as a potential modifier of Dravet syndrome. *PLoS Genet.* **5,** e1000649 (2009).
48. Hawkins, N. A., Zachwieja, N. J., Miller, A. R., Anderson, L. L. & Kearney, J. A. Fine Mapping of a Dravet Syndrome Modifier Locus on Mouse Chromosome 5 and Candidate Gene Analysis by RNA-Seq. *PLOS Genet.* **12,** e1006398 (2016).
49. Sun, L. *et al.* A knock-in model of human epilepsy in Drosophila reveals

a novel cellular mechanism associated with heat-induced seizure. *The Journal of neuroscience : the official journal of the Society for Neuroscience* **32,** 14145–14155 (2012).

50. Ananiev, G., Williams, E. C., Li, H. & Chang, Q. Isogenic pairs of wild type and mutant induced pluripotent stem cell (iPSC) lines from Rett syndrome patients as in vitro disease model. *PLoS One* **6,** e25255–e25255 (2011).
51. Bellin, M. *et al.* Isogenic human pluripotent stem cell pairs reveal the role of a KCNH2 mutation in long-QT syndrome. *EMBO J.* **32,** 3161–3175 (2013).
52. Du, X. & Parent, J. M. Using Patient-Derived Induced Pluripotent Stem Cells to Model and Treat Epilepsies. *Current neurology and neuroscience reports* **15,** 71 (2015).
53. Odawara, A., Katoh, H., Matsuda, N. & Suzuki, I. Physiological maturation and drug responses of human induced pluripotent stem cell-derived cortical neuronal networks in long-term culture. *Sci. Rep.* **6,** 26181 (2016).
54. Parent, J. M. & Anderson, S. A. Reprogramming patient-derived cells to study the epilepsies. *Nat. Neurosci.* **18,** 360–366 (2015).